

Analysis of fMRI Data Using Improved Self-Organizing Mapping and Spatio-Temporal Metric Hierarchical Clustering

Wei Liao, Huaifu Chen*, Qin Yang, and Xu Lei

Abstract—The self-organizing mapping (SOM) and hierarchical clustering (HC) methods are integrated to detect brain functional activation; functional magnetic resonance imaging (fMRI) data are first processed by SOM to obtain a primary merged neural nodes image, and then by HC to obtain further brain activation patterns. The conventional Euclidean distance metric was replaced by the correlation distance metric in SOM to improve clustering and merging of neural nodes. To improve the use of spatial and temporal information in fMRI data, a new spatial distance (node coordinates in the 2-D lattice) and temporal correlation (correlation degree of each time course in the exemplar matrix) are introduced in HC to merge the primary SOM results. Two simulation studies and two *in vivo* fMRI data that both contained block-design and event-related experiments revealed that brain functional activation can be effectively detected and that different response patterns can be distinguished using these methods. Our results demonstrate that the improved SOM and HC methods are clearly superior to the statistical parametric mapping (SPM), independent component analysis (ICA), and conventional SOM methods in the block-design, especially in the event-related experiment, as revealed by their performance measured by receiver operating characteristic (ROC) analysis. Our results also suggest that the proposed new integrated approach could be useful in detecting block-design and event-related fMRI data.

Index Terms—Correlation distance metric, functional magnetic resonance imaging (fMRI), hierarchical clustering analysis, self-organizing maps, spatio-temporal measure.

I. INTRODUCTION

FUNCTIONAL magnetic resonance imaging (fMRI), as a noninvasive imaging method based on the blood oxygenation level-dependent (BOLD) technique [1], [2], has emerged as a powerful tool used in numerous experiments to identify

those regions of the brain associated with specific cognitive processes. Its high temporal and spatial resolution enable it to be used as a potential method of mapping rapid and fine activation patterns of the human brain [1]–[5]. Two types of experimental paradigms are prevalent in current fMRI research. In a block-design experiment, the subject is exposed to prolonged stimulus or asked to execute a task repeatedly in alternation with a control and a task condition over a period of time. In contrast, an event-related experiment [6], [7] requires the subject to perform a task in a single instance while the corresponding transient response is measured. To find the response waveforms and localize the brain activation associated with the task, a large number of models and techniques have been widely used, including signal processing and statistics [3]–[6]. At present, the primary approach to fMRI data analysis can be generally divided into two types, depending on whether prior knowledge is required regarding the experimental paradigm: hypothesis- and data-driven approaches.

Several types of statistical tests have been used in the hypothesis-driven approach [8]. Statistical parametric mapping (SPM) [9] based on the general linear model (GLM) [10] and the non-parametric Kolmogorov–Smirnov test [11] are powerful tools for analyzing fMRI data; however, these methods require determinate statistical inference and hypothesis tests. Similarly, as statistical test methods, *t*-tests and the *F* test require accurate time information that corresponds to the experiment pattern to compute the temporal correlation between the reference pattern and the observed BOLD signals [12], [13]. An improved model based on the adjusted R-square has been processed to assess and build the model in fMRI [14]. These methods have been the most widely used, especially in block-design experiments, because they provide some statistical inferences; these approaches have revealed that the brain response to a specific stimulus or a task is approximately equal to the convolution of the paradigm with the hemodynamic response function (HRF) [15]–[17]. It is crucial to gain an understanding of the underlying dynamics of brain activation [18], [19] when analyzing single trial data or event-related experiments where the actual and robust response is complex rather than providing irrefutable confirmation [20], [21]. Thus, the deconvolution [22] and the Bayesian methods [23] are employed to deal with this problem.

Hypothesis-driven studies, which do not fully embody the brain activation process, take advantage of external inferences only; conversely, they do not adequately take account of the internal relationships in fMRI data. Hence, data-driven techniques would greatly facilitate the processing of fMRI

Manuscript received January 15, 2008; revised March 26, 2008. First published April 22, 2008; current version published September 24, 2008. This work is supported in part by the Natural Science Foundation of China (NSFC), under Project 30570507, Project 30770590, and Project 2003CB716100, in part by the New Century Excellent Talents in University under Grant NCET-05-0809, in part by the key research project of science and technology of Ministry of Education (MOE) under Grant 107097 and 863 Program 2007AA02Z430. Asterisk indicates corresponding author.

W. Liao, Q. Yang, and X. Lei are with School of Life Science and Technology, School of Applied Math, University of Electronic Science and Technology of China, Chengdu 610054, China.

*H. Chen is with School of Life Science and Technology, School of Applied Math, University of Electronic Science and Technology of China, Chengdu 610054, China (e-mail: chenhf@uestc.edu.cn).

Color versions of one or more of the figures in this paper are available online at <http://ieeexplore.ieee.org>.

Digital Object Identifier 10.1109/TMI.2008.923987

data for certain given conditions. Several types of data-driven approaches—those that do not require any prior assumption regarding the task paradigm—have been introduced for fMRI data analysis. Here, they are utilized in functional task experiments in the context of principal component analysis (PCA) [24], [25] or independent component analysis (ICA) [26]–[28]. The major problem of PCA is that it only diminishes second-order dependency between each component and it is assumed that each component is mutually orthogonal; however, the question of whether the physiological meanings of these components are mutually orthogonal remains unanswered. ICA can reduce higher-order dependency, but it is still limited in selecting expected components from a number of components [29].

Cluster analysis, another data-driven method, includes K-means methods analysis [30], fuzzy cluster analysis [31], hierarchical clustering (HC) analysis [32], [33], and self-organizing mapping (SOM) [34]–[38] of group image voxels into clusters using the similarity of their time course based upon the assumption that the pattern of activation has a structure and can be divided into several types of similar activations [32]. The data analyst can then inspect the resulting clusters to identify interesting temporal patterns [37].

Kohonen's SOM [39]–[41], of which the principal goal is to transform an incoming signal pattern of arbitrary dimension into a 1-D or 2-D discrete map and to perform this transform adaptively in a topologically ordered fashion, can also be employed in clustering fMRI data. To map a high-dimensional signal intensity space to “neurons” of 2-D lattice space, there should be a sufficient number of nodes used in the SOM algorithm to ensure adequate flexibility and mapping quality. Accordingly, several approaches have been developed that cluster the SOM weights and assign them to the cluster of prototype vector to which they map, thus providing automated cluster extraction. Thus, there are many details that determine the quality of the resulting clustering, especially for fMRI data.

A hierarchical classification based on the Ward measure obtains superclusters from the SOM weights [42]. Merging neighboring nodes with least mutual distance based on contiguity-constrained clustering [43] have been introduced in [34] and [36] furnishes using a fuzzy c-means method to cluster the SOM weights, while a method called node merging, which is utilized to merge SOM nodes whose feature vectors are sufficiently similar to another, has been proposed in [37]. A generating supercluster method, which was formed by finding the minimum least-squares distance between each exemplar time course and those of its immediate neighbors, is proposed to analyze functional connectivity in fMRI data [38]; however, in conventional SOM and HC the simple Euclidean distance is most commonly used because it does not denote the spatial and temporal information for fMRI data at the same time.

In the present study, the SOM and HC methods are integrated to detect brain functional activation; fMRI data are first processed by SOM to obtain a primary merged neural nodes image before being processed by HC to obtain further brain activation patterns. Because of the fMRI baseline effect, in first-step algorithms of SOM another similarity measure (correlation distance metric) is calculated between the input fMRI time course signal and the exemplar time course (weights) of the lattice node. A

new spatio-temporal measure in hierarchical clustering is introduced in second-step algorithms, taking into consideration the fact that the weights in the node not only denote spatial coordinates in the lattice but also imply temporal information regarding these weights. Improved SOM and spatio-temporal hierarchical clustering approaches are presented in Section II, while simulation data and fMRI experiments are presented in Section III. The simulation and in vivo fMRI results are discussed in Sections IV and V.

II. METHODS AND DATA

A. Kohonen Self-Organizing Map

SOM, as proposed in [44] and used thoroughly in fMRI data processing in [34]–[36] and [38], is one of the foremost unsupervised artificial neural network models, as well as an exploratory tool for fMRI data analysis.

Basically, the SOM network consists of a set of units i arranged according to a topology for which the most common choice is a 2-D grid lattice. In the present paper, we let $i = 100$ and arranged the 100 exemplars into a 10×10 2-D grid lattice. Each of the units is assigned a weight vector m_i of the same dimension as the input data $m_i = [m_{i1}, m_{i2}, \dots, m_{in}]^T \in \mathbb{R}^N$. The length N is equal to the length of the fMRI time course. In the initial setup of the model prior to training, the weight vectors might be filled with random values, as in the above-mentioned contributions; however, here the initial values of m_i are preferably selected at random from a time course of a volume that came from the domain of the input samples. In the following expression, we make use of a discrete time notation, with t denoting the current training iterations. In one iteration, the time course of every voxel as an input pattern $x(t)$ is randomly selected from the set of input vectors—the time course of all voxels. Commonly, the activity level of a unit is based on any metric between input vectors x compared with all the exemplar time courses m_i . For example, in many practical applications the smallest Euclidean distance $\|x - m_i\|$ can be made to define the best matching node [34]–[38]. Nevertheless, given that the input vector x and exemplar time course m_i both denote the fMRI time course, the correlation distance metric reveals their similarities better than the conventional Euclidean distance metric.

Consequently, the selection of the winner node c may be written as given in

$$m_c(t) = \arg \max_i \{\text{corr}(x(t), m_i(t))\}, i = 1, \dots, M \quad (1)$$

where $x(t)$ is the time course of the data voxels under consideration, $m_i(t)$ denotes the time course of exemplar i , $m_c(t)$ is the time course of the closest exemplar c , and M is number of exemplars. $\text{corr}(x(t), m_i(t))$ are the normalized correlation coefficients (CCs) between $x(t)$ and $m_i(t)$.

The exemplars are then updated at each iteration using

$$m_i(t+1) = m_i(t) + h_{ci}(t) \cdot [x(t) - m_i(t)] \quad (2)$$

where t is the current learning iteration, $t = 0, 1, 2, \dots$ is an integer (the discrete-time coordinates), and the function $h_{ci}(t)$

represents the time-varying neighborhood-kernel. The neighborhood units around the winner node may be described implicitly by means of a neighborhood-kernel $h_{ci}(t)$ that takes into account the distance—in terms of the output space—between the exemplar time course i under consideration and c . The smoother neighborhood-kernel widely applied can be written in terms of the Gaussian function

$$h_{ci}(t) = \alpha(t) \cdot \exp \left\{ -\frac{\|r_c - r_i\|^2}{2\sigma^2(t)} \right\} \quad (3)$$

where $\alpha(t)$, which varies with learning iteration t , is a learning rate that controls how fast the exemplar changes, set as 0.1; $\|r_c - r_i\|$ denotes the distance between exemplar c and i within the output space (i.e., in the 2-D exemplar matrix); and $\sigma(t)$ defines the full-width at half-maximum (FWHM) of the Gaussian kernel. We set the initial size $\sigma(0)$ of the neighborhood function equal to the “radius” of the lattice. In the present study, we initiated seven nodes as a “radius,” as in a previous study [38]. At each iteration step, the learning rate $\alpha(t)$ decreases gradually by $t/100$ ($100 = \text{total iterations}$) exponential decay as the learning iteration t increases; $\sigma(t)$ decreases gradually by exponential decay as the learning iteration t increases. The time courses of those voxels within the brain in each slice as the input vector $x(t)$ were compared with the exemplar map, as mentioned above. In general, a total of 100 iterations are sufficient to establish convergence of the algorithm. When the 100 iterations had completed through SOM algorithm, the 100 exemplars was generated. So each exemplar has one time course. Every voxel within the brain in each slice is assigned to one of the 100 exemplars if the CC that computed between the voxel’s time course and that exemplar’s time course is maximal, and that maximal CC illustrated the degree of the voxel belongs to that exemplar.

B. Spatio-Temporal Hierarchical Clustering

The SOM algorithm was used to generate a set of exemplars for each data set. After SOM training, a group of similar exemplar time courses was identified and all voxel time courses assigned into the cluster of their prototype vector. Without doubt, the SOM method can successfully cluster the high-dimensional fMRI data sets into a 2-D lattice space. If we regard the exemplar (100 exemplars in this study) as a cluster, there would be too many clusters to explain; however, the use of 100 nodes (exemplars) results in better optimization than that obtained using smaller or larger nodes [38]. At the same time, clustering the SOM weights is of particular interest because it has great potential in terms of both finding detailed structure and providing a high level of automation. Various methods for clustering SOM weights have been proposed [34]–[38], [45], [46]. Thus, to enable effective utilization of the information provided by the SOM, methods are required that provides good candidates for mapping units into clusters or groups. The reasons of choosing hierarchical clustering are: 1) unlike the number K of clusters must be specified in advance of K-means algorithm [32], [33]. 2) It should be emphasized that the goal here is not to find an optimal clustering for the data, but to obtain clear insight into the cluster structure of data;

in particular, in fMRI data analysis. Because fMRI data is a dataset that includes spatio-temporal information, the exemplar matrix (nodes of the lattice), which has been generated by the SOM approach, should consist of temporal information that corresponds to $m_i(t)$ and spatial information that corresponds to exemplars that are topologically ordered, which means that exemplars have individual coordinates in the lattice. Therefore, the clustering method should be fast, robust, and visually efficient. We defined a new measure of spatio-temporal distance between two exemplar time courses as

$$d_{ST} = \text{corr}(m_i(t), m_j(t)) \cdot \exp \left\{ -\frac{\|r_i - r_j\|^2}{2\sigma^2} \right\} \quad (4)$$

where $\|r_i - r_j\|$ is the Euclidean spatial distance between exemplars m_i and m_j (details are provided in Section II-A), $\text{corr}(m_i(t), m_j(t))$ are the normalized CCs between the time sequences of exemplars m_i and m_j , and σ is the FWHM of the Gaussian function. Measurement in (4) is based on spatial neighborhood and temporal correlated activation, and may be in accordance with the physiological fact that neighborhood neuronal activation should show a similarity [33]. On this basis, the spatio-temporal distance mentioned above is defined as the within-cluster distance in the merging criterion, and single linkage is defined as the between-cluster distance in the linkage option. HC was only used in clustering the 100 exemplar matrix (nodes of the lattice) generated by the SOM approach.

C. Performance-ROC Analysis

To validate the performance of our method and compare it with the SPM and ICA [26] methods, we performed receiver operating characteristic (ROC) analysis [47]. The false-positive ratio (FPR), being the number of misclassified inactivated voxels divided by the total number of voxels considered, and the true positive ratio (TPR), being the number of correct classifications of activated voxels divided by the total number of voxels considered, are defined as the x axis and the y axis in the ROC curve, respectively [48]. To plot the ROC curve for SPM and ICA analysis methods [26], we varied the threshold of SPM without an FWE-corrected from $p\text{-value} = 0.001$ to 0.05, and with an FWE-corrected $p\text{-value} = 0.001$ to 0.05, and the threshold of ICA from $|Z|$ value $= 2.0$ ($p = 0.05$) to 6.0 ($p = 0.001$) [28]. And based on the previous study [36]: a higher threshold, tended to have a higher value of specificity and a lower value of sensitivity. The conditions closest to the left upper corner of ROC curves, based on the ideal value of TPR and FPR is one, any curve corresponding to a certain method closest to the ideal upper left corner of a ROC plot will be the method of choice. So, in our method, the threshold, following [36], was chosen to be the output cluster number, which was varied from 2, 3, \dots , 8.

We then calculated the correlation between the centers of the identified activation clusters (the supercluster time course) and the reference activation class (the different experiment paradigm) [46]. The CC should exhibit the quality and delay points of the cluster represented by its center towards that of the reference. Note that the CC is used for both simulation data and in real fMRI.

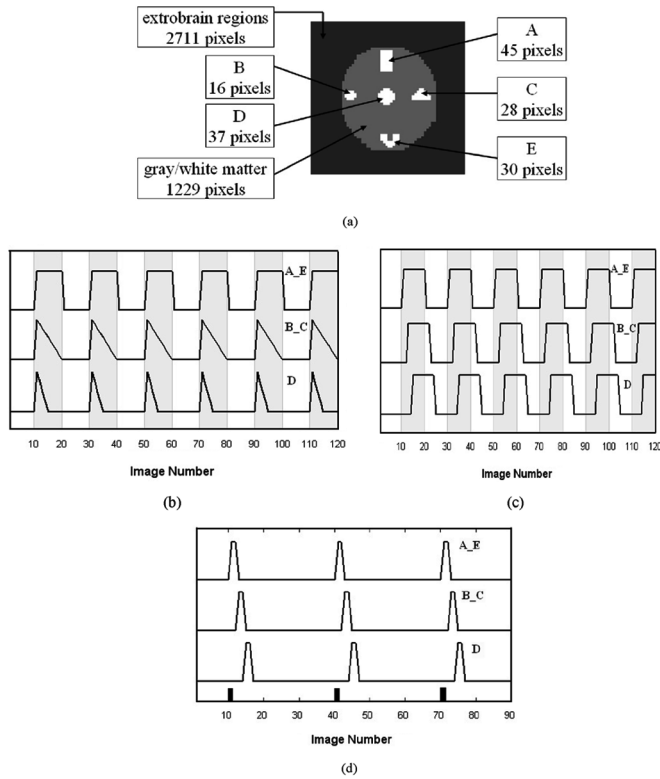


Fig. 1. Schematic illustration showing spatial and temporal patterns in synthetic fMRI datasets. (a) Spatial distribution of assumed active voxels. (b) Three assumed stimulation patterns with 10 points at rest and 10 points at task conditions in BS1. (c) Three assumed stimulation patterns in BS2. (d) Three assumed stimulation patterns of event-related simulation in BS4.

D. Generation of Simulated Data

In the present study, two synthetic fMRI images (64×64 voxels) were generated, including block-design and event-related experiments. Fig. 1(a) displays five active subregions (156 voxels) with a time-invariant margin of 2711 voxels and a stochastic variant texture of 1229 voxels (gray/white matter, ventricles).

1) *Block-design Experiment*: The three block-design synthetic datasets, BS1–BS3, were composed of five active subregions using activation patterns embedded at known locations. Dataset BS1 was designed to illustrate variability in the shape of the hemodynamic response to a stimulation block. Three different hemodynamic responses were added to subregions “A” and “E” (“A_E”), subregions “B” and “C” (“B_C”), and subregion “D” [see Fig. 1(b)]. The subregions “A” and “E” (“A_E”), whose spatial pattern was remote and whose temporal pattern was accordant, were merged into one homogeneous active source. In the same sense, the subregions “B” and “C” (“B_C”) were merged in our study. The time series of all the voxels of a subregion consist of the given signal mixed with Gaussian noise under contrast-noise-ratio (CNR) = 2.0 (CNR is defined as the amplitude of the normalized ideal waveform is divided by the standard deviation of the noise). The supposed box-car-like signal is shown in the first row of Fig. 1(b).

BS2 was designed to illustrate timing variability between the stimulation paradigm and hemodynamic response (activation

delay). Three active temporal patterns with three delayed versions (delay of 0, 4, or 8 s) [Fig. 1(c)] of the aforementioned “expected” boxcar-like timing function are depicted in the first row of Fig. 1(c). The spatial pattern and CNR were identical to those of BS1.

BS3 was designed to illustrate signal-to-noise variability. Only one activation source (subregions “A” and “E” (“A_E”)) was associated with the aforementioned ‘expected’ boxcar-like timing function as a temporal pattern [first row of Fig. 1(b)]. The differences in CNR (0.5, 1.0, 1.5, 2.0, and 2.5) were calculated repeatedly.

2) *Event-Related Experiment*: The two event-related synthetic datasets, BS4 and BS5, were composed of five active subregions using activation patterns embedded at known locations.

BS4 was designed to illustrate timing variability between the stimulation paradigm and hemodynamic response (activation delay) in event-related datasets. Three active temporal patterns with three delayed versions (delay of 0, 4, or 8 s) [Fig. 1(d)] of the aforementioned ‘expected’ boxcar-like timing function are depicted in the first row of Fig. 1(d). A practical event stimulus pattern, such as that in the first row in Fig. 1(d), was used in the actual event-related fMRI data collection. The spatial pattern and CNR were identical to those of BS1.

BS5 was designed to illustrate signal-to-noise variability in event-related data sets. Only one activation source (subregions “A” and “E” (“A_E”)) was associated with the aforementioned ‘expected’ boxcar-like timing function as a temporal pattern [first row of Fig. 1(d)].

E. Experimental Paradigm

1) *Block-Design Experiment*: An *in vivo* fMRI multitask block-design experiment was performed using visual stimulus and synchronous hand movement. The condition for successive blocks alternated between rest and simultaneous visual stimulus and hand movement, starting with rest. Visual stimulation was presented at the center of the visual field with a frequency of 8 Hz, light intensity of 200 cd/cm², and visual angle of 2°. Visual stimulation signals acted as a trigger to start hand movement.

Three healthy subjects participated in the fMRI experiment (two males, one female; mean age, 30 years). The experiment was conducted at the University of Texas Health Center, San Antonio, using a 3-T Magnetom TRIO (Siemens). Gradient echo EPI sequences were acquired using the following parameters: 23 slices; TR, 2000 ms; TE, 40 ms; FOV, 24 cm; matrix, 64×64 ; in-plane resolution, 3.75×3.75 mm; flip angle, 90°. A total of six cycles (12 epochs) were performed, as shown for first row in Fig. 1(b); thus, 120 scans were acquired.

2) *Event-Related Experiment*: Each subject attended two sessions in this experiment. One session was a motor event-related experiment that presented stimulus three times, at 20, 80, and 140 s; each stimulus was presented for a period of 2000 ms. The other time was a blank trial, with only the center fixation cross (0.8°) displayed. Subjects were required to concentrate on the fixation cross and start the movement using two hands when the stimulus began.

The other session was a visual event-related experiment. Each subject performed a visual event-related experiment that presented stimulus three times, at 20, 80, and 140 s; each stimulus was presented for a period of 2000 ms. A blank trial was also performed in which the stimulus was presented at the center of the visual field, with a frequency of 8 Hz, light intensity of 200 cd/cm² and visual angle of 2°. Gradient echo EPI sequences parameters were identical with block-design experiment. The paradigm reference was shown as first row in Fig. 1(d); thus, 90 scans were acquired.

F. Data-Processing Procedure

First, the experimental data were analyzed using SPM2 software¹ [49], [50]. To detect gross head movement in all data, spatial transformation that included realignment was performed using 3-D rigid-body registration to correct for head motion.

Second, to increase analysis efficiency, only signals in the brain were processed. Voxels with values lower than a certain threshold were regarded as background. Empirically, we set the threshold values to be 1/10th of the highest intensity in the input image [36].

Third, we systematically removed noise from the considered data after eliminating background noise from the fMRI data. Linear trends were removed from the data to eliminate the effect of gross signal drifts, which could be caused by scanner instabilities and/or gross physiological change in the subject. A high-pass filter with a cutoff of 1/128 Hz was used to remove low-frequency noise. Many previous papers consider that each time course can be normalized by subtracting its mean and dividing by its standard deviation, to give a time course with zero mean and unit variance before using SOM [37], [38]. Because the fMRI signal intensity information is significant in clustering or classifying the fMRI data, we did not normalize the fMRI signal in the following analysis. Finally, the data were processed by SOM followed by spatio-temporal hierarchical clustering. The initial parameters in the SOM were as follows: initial learning rate [in (3)] $\alpha(0) = 0.1$; initial size [in (3)] $\sigma(0) = 7$; learning iteration $t = 0, 1, 2, \dots, 100$, and the number of total iterations was set at 100 for both the simulated and real data. And, the Gaussian function σ [in (4)] was set at 4 in the simulated data and 8 in the real data.

III. RESULTS

A. Simulation Test

1) *Block-Design Experiment*: Fig. 2(a) shows the ability of an integrated improved SOM and spatio-temporal hierarchical clustering (STHC) technique to identify winner nodes, merge the nodes, and generate an exemplar time course for activation detection in BS1. Fig. 2(a) shows the exemplar matrix (100 nodes) resulting from our method. Different colors are used to demonstrate the fact that each colored exemplar time course denotes a corresponding activation pattern. Fig. 2(b) shows the stimulation brain activation of SPM analyses results thresholded without an FWE-corrected p -value < 0.001 and thresholded

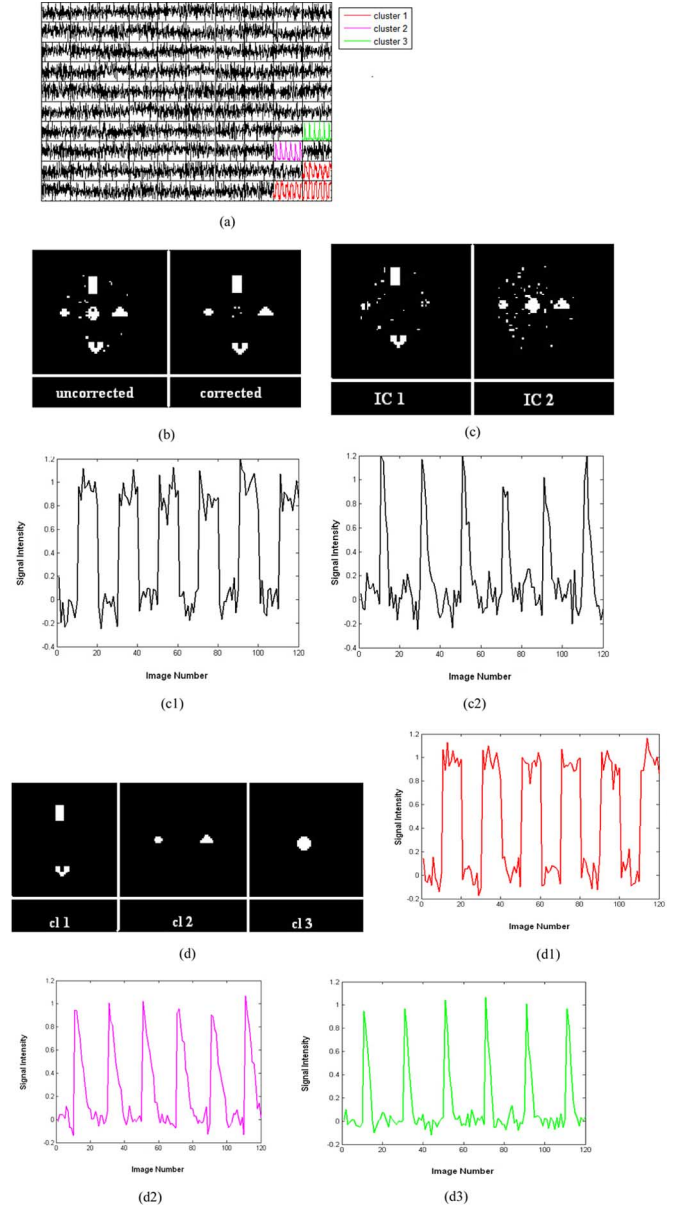


Fig. 2. Results of BS1 under CNR = 2.0. (a) Resultant exemplar time course matrix after applying the SOM algorithm to the simulation test in the block-design dataset. Differently colored time courses correspond to different superclusters. (b) SPM activation map thresholded without an FWE-corrected p -value < 0.001 and thresholded with an FWE-corrected p -value < 0.05 , respectively. (c) ICA activation map ($|Z| > 3.0$); the two temporal components are shown in (c1) and (c2), respectively. (d) Activation regions computed by our method. (d1)–(d3) Averaged exemplar time courses corresponding to the respective brain activation patterns shown in (d). cl = cluster.

with an FWE-corrected p -value < 0.05 , respectively. Fig. 2(c) shows stimulation brain activation, including two independent spatial activation maps computed by the ICA. These two independent components (which correspond to the temporal components) are plotted in Fig. 2(c1) and (c2). The details of the three different simulated brain activation areas (BS1) that were described in Section II-D can be clustered into three individual clusters that were expected to be active [Fig. 2(d)]. At the same time, one supercluster exemplar time course was averaged by a single or several exemplar time courses of one cluster in the 2-D lattice [Fig. 2(d1)–(d3)].

¹<http://www.fil.ion.ucl.ac.uk/spm>

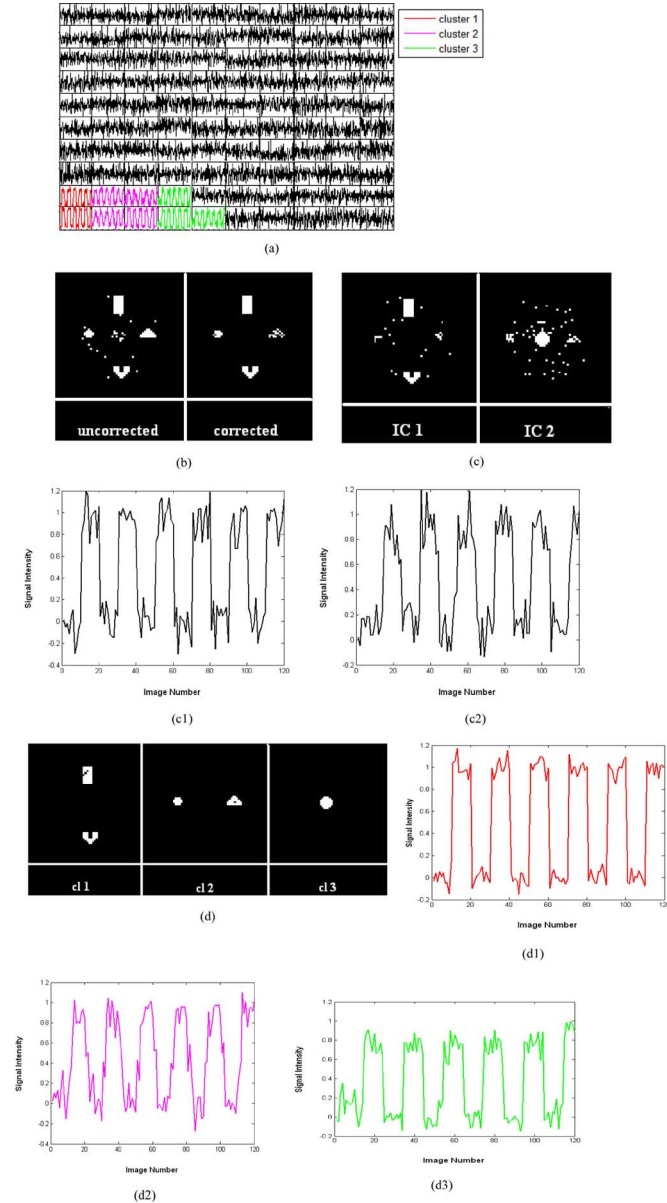


Fig. 3. Results of BS2 under $\text{CNR} = 2.0$. (a) Resultant exemplar time course matrix after applying the SOM algorithm to BS2. Differently colored time courses correspond to different superclusters. (b) SPM activation map thresholded without an FWE-corrected p -value < 0.001 and thresholded with an FWE-corrected p -value < 0.05 , respectively. (c) ICA activation map ($|Z| > 3.0$); the two temporal components are shown in (c1) and (c2). (d) Activation regions computed by our method. (d1)–(d3) Averaged exemplar time courses corresponding to the respective brain activation patterns shown in d. cl = cluster.

The results of BS2 that illustrate timing variability between the stimulation paradigm and hemodynamic response (activation delay) are shown in Fig. 3, including the results of SPM, ICA, and our method.

BS3 was designed only to illustrate signal-to-noise variability in the block-design dataset. The activation maps computed by the various methods are not shown. The performances of the various methods are analyzed in Section III-C.

2) *Event-Related Experiment*: The results of BS4 that illustrate timing variability between the stimulation paradigm and hemodynamic response (activation delay) for the event-related

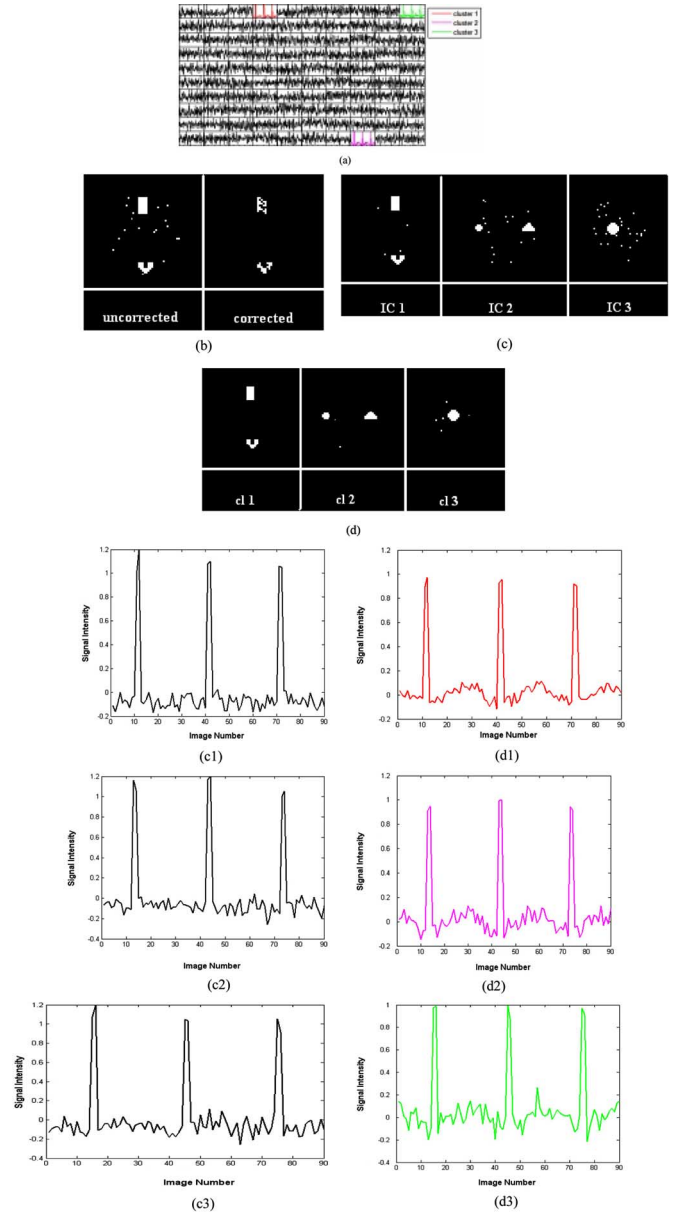


Fig. 4. Results of BS4 under $\text{CNR} = 2.0$. (a) Resultant exemplar time course matrix after applying the SOM algorithm to BS4. Differently colored time courses correspond to the different superclusters. (b) SPM activation map thresholded without an FWE-corrected p -value < 0.001 and thresholded with an FWE-corrected p -value < 0.05 , respectively. (c) ICA activation map ($|Z| > 3.0$); the three temporal components are shown in (c1)–(c3). (d) Activation regions computed by our method. (d1)–(d3) Averaged exemplar time courses corresponding to the respective brain activation patterns shown in (d). cl = cluster.

dataset are shown in Fig. 4, which includes results obtained using SPM, ICA, and our method.

BS5 was designed only to illustrate signal-to-noise variability in the event-related dataset. The activation maps computed by the various methods are not shown. The performances of the various methods are analyzed in Section III-C.

B. Actual fMRI Experiment Data Test

1) *Multitask Block-Design Experiment*: Visual stimulation and synchronous hand movement were performed in this paradigm. Although these tasks were performed synchronously, the

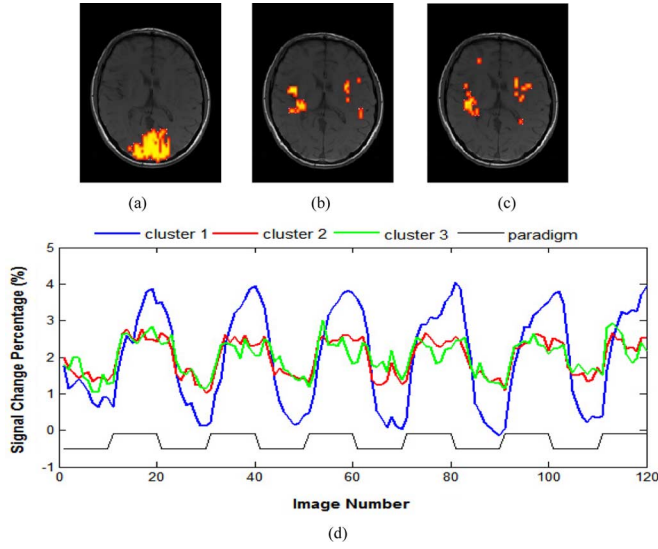


Fig. 5. Results in the visual cortex for the real fMRI test of the multitask block experiment. (a) Activation areas located in the primary visual areas. (b) and (c) Activation areas located in the motor areas. (d) Signal changes of three different supercluster time courses are colored differently, while the experiment paradigm is colored in black.

responses of the brain neurons to this task may occur at different times, as the visual response is dissimilar to the motor response. The results of conventional methods such as correlation analysis and t -test in using the paradigm as a reference signal would introduce bias in this experiment; however, the SOM technique did not use the paradigm as the reference signal, and is thus adapted to a multitask experiment. Fig. 5(a)–(c) shows three different activation patterns that correspond to this task. One activated area [Fig. 5(a)] is the primary visual area that responded to the visual stimulations. Fig. 5(b) and (c) reveals that some activated areas are located in the motor areas, and Fig. 5(d) demonstrates the three different supercluster time courses and the experiment paradigm.

In the multitask experiment that consisted of visual stimulus and hand movement, we observed region activation in another slice that mainly contains the primary motor cortex. Other areas of brain activation are possible connectivity clusters, with separated clusters found in spatially distinct regions [38], as shown in Fig. 6.

2) *Visual and Motor Event-Related Experiment*: In this section, we consider visual and other motor event-related exemplars. Fig. 7(a) and (b) demonstrates the results of the SOM algorithm that typically detected brain activation in the primary visual cortex, which corresponds to the supercluster time courses plotted in Fig. 7(e) and (f), respectively. The other possible connectivity clusters that corresponded to these brain activation areas and supercluster time courses are shown in Fig. 7(c) and (d) and Fig. 7(g) and (h), respectively.

We then considered the primary motor cortex. Fig. 8(a)–(d) shows the brain activation areas in the bilateral motor cortex and primary motor cortex and other possible connectivity areas. The supercluster time course corresponding to the activated areas is shown in Fig. 8(e)–(f).

The fMRI BOLD signal showed relatively little change with stimulus in the event-related experiment compared to the block-

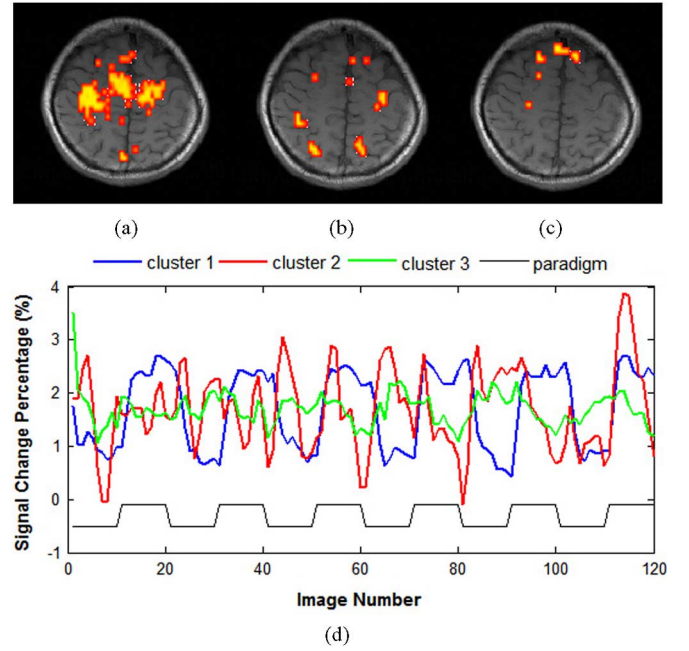


Fig. 6. Results in the motor cortex for the real fMRI test of the multitask block experiment. (a) Activation areas are located in the primary motor areas. (b) and (c) Activation areas reveal possible connectivity. (d) Signal changes of three different supercluster time courses are colored differently, with the experiment paradigm shown in black.

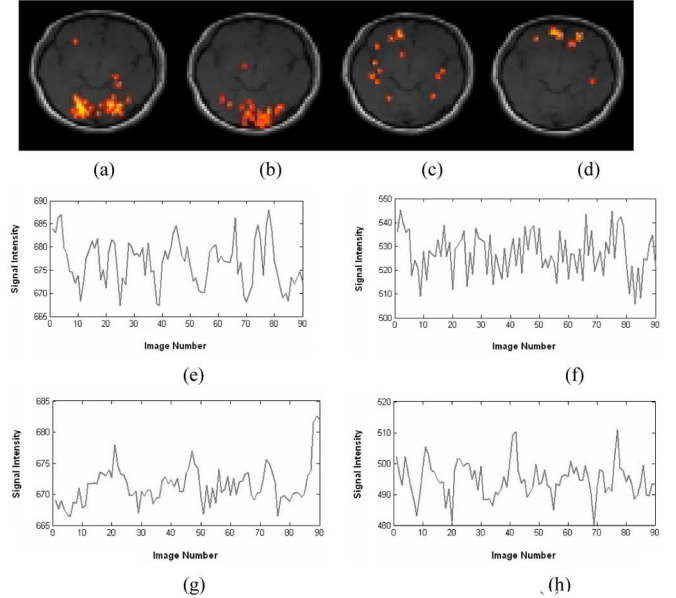


Fig. 7. Results in the visual cortex for the real fMRI test of the visual event-related experiment. (a) and (b) Activation areas are in the primary visual cortex. (c) and (d) Activation areas reveal possible connectivity. (e)–(h) Signals of the four different supercluster time courses are colored differently, corresponding to the four activation patterns.

design fMRI experiments. Therefore, CNR is a key factor in the analysis of the fMRI data set, especially in conventional correlation coefficient analysis and t -test methods that depend on the statistical significance of the time course and paradigm reference.

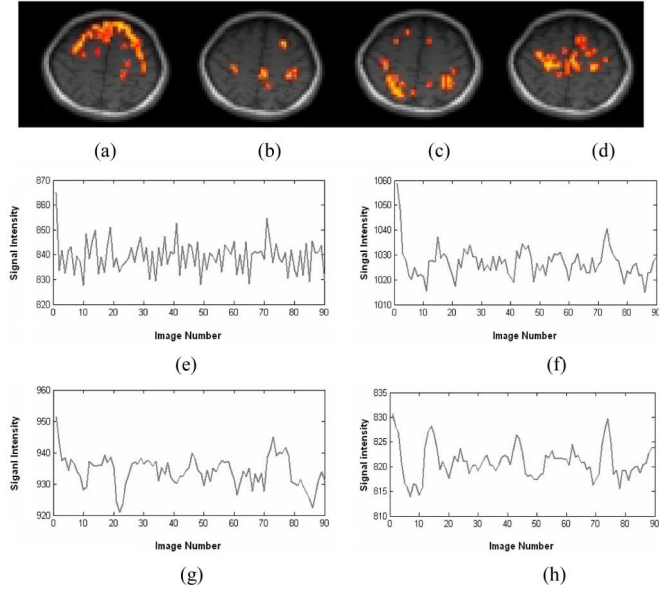


Fig. 8. Results in the motor cortex for the real fMRI test of the motor event-related experiment. (a)–(d) Activation areas computed by the SOM. (f)–(h) Signals of four different supercluster time courses are colored differently corresponding to the four activation patterns.

C. Results of Performance-ROC Analysis

ROC analysis was performed to validate the performance of our method and to enable comparison with the SPM and ICA methods. ROC curves for BS1–BS5 are plotted in Fig. 9(a)–(e), respectively. Fig. 9(f) shows the ROC curve calculated by the conventional SOM using the Euclidian distance metric, and our improved SOM using the correlation distance metric under different CNR conditions (0.5, 1.0, 1.5, 2.0, and 2.5). Only one activation source (subregions “A” and “E” [“A_E”]) was associated with the aforementioned “expected” boxcar-like timing function as a temporal pattern [first row of Fig. 1(b)]

We also calculated the CC between temporal components computed by ICA and the supercluster time courses computed by our method and the reference time courses that assumed brain activation patterns. Table I shows CC computed for BS1, BS2, and BS4 in the stimulation test; “cl” denotes the cluster, and “A_E,” “B_C,” and “D” denote the reference time courses that were derived from those subregions. Table II shows CC computed for the multitask block-design and visual and motor event-related experiments in the real fMRI test.

IV. DISCUSSION

A. Metric Selection in SOM

Many reports [34]–[38] have used the SOM algorithm in clustering fMRI data and utilized the Euclidean distance metric to select the best-matching node. In the present study, we applied the correlation distance metric as the criterion for selecting the winner node. This was done for two main reasons. First, the task and the control fMRI signal have different baseline levels for block-design and event-related fMRI data, which are dissimilar to the resting fMRI data signal intensity for the same level. The

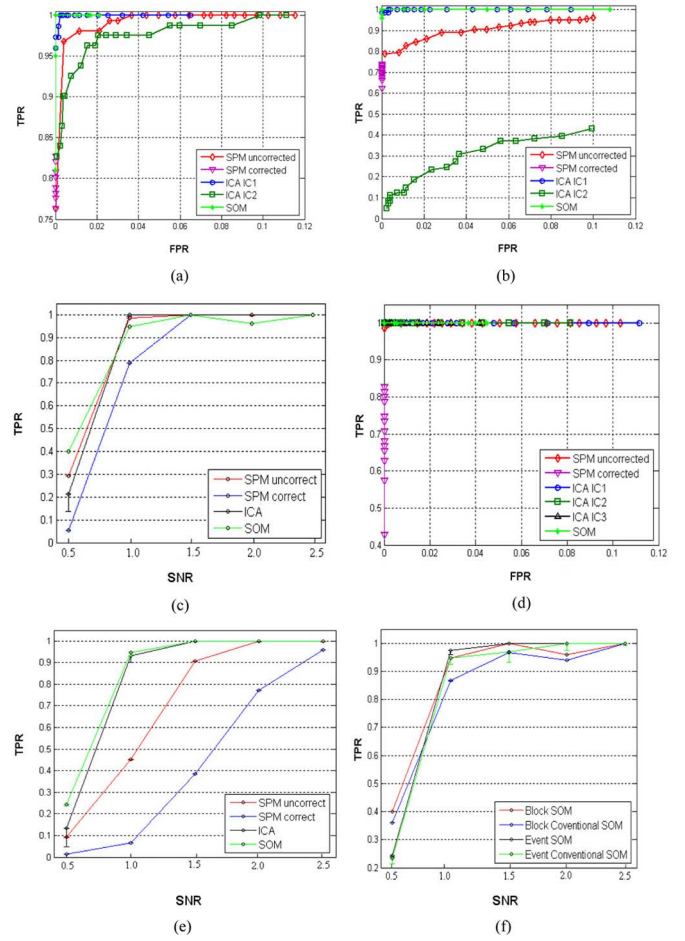


Fig. 9. ROC curves of BS1–BS5 (a)–(e). (f) Comparison of the performance of conventional SOM (Euclidian distance metric) and our improved SOM (correlation distance metric) for block-design and event-related simulation datasets. Only one activation source (subregions “A” and “E” [“A_E”]) was associated with the aforementioned “expected” boxcar-like timing function as a temporal pattern [first row of Fig. 1(b)]. Vertical bars in (c), (e), and (f) indicate estimated FPR.

Euclidean distance depends on calculating the distance between two discrete points, which may be large if the signal intensity of the two time courses is not the same at the baseline level. Second, the time course in the actual fMRI signal can exist at one or more singular points (noise points), leading to a larger Euclidean distance than that expected. In other words, the Euclidean distance metric in the SOM algorithm does not accurately reflect the interference of the noise points. Naturally, the correlation distance metric is better than Euclidean distance for the SOM algorithm in task-condition fMRI data.

Fig. 9(f) shows that using the correlation distance metric could result in a higher TPR than that for Euclidean distance under different CNR levels. The activation map including the block-design and event-related stimulation test further proves the detection ability of the new method. Fig. 2(d) illustrates an activation map without any noise points detected by the correlation distance metric SOM in the block-design experiment. Fig. 4(d) illustrates an activation map with noise points detected by the correlation distance metric SOM in the event-related experiment.

TABLE I
CC ANALYSIS RESULTS OF BS1, BS2 OF BLOCK-DESIGN AND BS4 OF EVENT-RELATED EXPERIMENTS IN THE SIMULATION TEST

	BS1			BS2			BS4		
ICA	IC 1	IC 2		IC 1	IC 2		IC 1	IC 2	IC3
	0.9739 (A_E)	0.8681 (B_C)/ 0.9277 (D)		0.9653 (A_E)	0.6792 (B_C)/ 0.9445 (D)		0.9706 (A_E)	0.9821 (B_C)	0.9855 (D)
Our method	cl 1	cl 2	cl 3	cl 1	cl 2	cl 3	cl 1	cl 2	cl 3
	0.9847 (A_E)	0.9880 (B_C)	0.9856 (D)	0.9925 (A_E)	0.9082 (B_C)	0.9636 (D)	0.9763 (A_E)	0.9449 (B_C)	0.9633 (D)

TABLE II
CC ANALYSIS RESULTS OF MULTITASK BLOCK-DESIGN AND VISUAL AND MOTOR EVENT-RELATED EXPERIMENTS IN THE STIMULATION TEST. CC RESULTS CONTAIN THE MAXIMUM CC AND THE DELAY SAMPLE POINT. VARIOUS CLUSTERS ARE SHOWN IN THE ABOVE RESULTS

	block-design						event-related							
	Slice 12			Slice 18			Slice 9				Slice 18			
	cl 1	cl 2	cl 3	cl 1	cl 2	cl 3	cl 1	cl 2	cl 3	cl 4	cl 1	cl 2	cl 3	cl 4
CC	0.878 5 (3)	0.902 5 (2)	0.692 9 (2)	0.896 4 (2)	0.383 1 (6)	0.476 8 (5)	0.222 1 (4)	0.245 2 (4)	0.272 6 (6)	0.390 7 (6)	0.368 3 (3)	0.334 9 (3)	0.212 9 (6)	0.385 0 (3)

B. Distance Measure Selection in STHC

In clustering the output weights (exemplar matrix) of the result of SOM into a specific cluster (supercluster), we utilized a spatio-temporal measure as the within-cluster distance to more accurately obtain a supercluster for visualization of the clustering results. For comparison, in other clustering approaches the SOM method alone is employed. Replacing the prior spatio-temporal distance d_{ST} by another hierarchical cluster and retaining all other conditions, the algorithm failed to cluster the regions in Fig. 2(a), Fig. 3(a), and Fig. 4(a) into three individual patterns. This finding means that d_{ST} is superior to the simple Euclidean distance (which denotes the similarity of two voxels in fMRI) when we need to take spatial and temporal information into consideration synchronously. The inherent feature of the SOM algorithm is that output weights are topologically ordered. Clearly, the exemplar time course and other exemplar time courses with high CCs in its vicinity should be grouped into a supercluster. Our simulation and the actual fMRI data results show that the new spatio-temporal distance measure successfully categorized all voxels into activation regions [Fig. 2(a), Fig. 3(a), and Fig. 4(a)] and noise (not shown).

C. Classifying Different Intensities in fMRI

The time courses of different brain regions have simultaneous responses to an identical task or instantaneous stimulus. Conventional SPM, as well as correlation coefficient analysis and the t -test, can distinguish these activation areas from other non-activated brain areas. Fig. 10(a) shows that the activation map computed by SPM consists of two main activation areas: the primary visual cortex and the bilateral motor cortex. Although this method can identify the voxels of these areas that have synchronal response to our paradigm, it cannot uncover the relationship between the two activation areas. Fig. 10(b) shows that the activation map computed by ICA consists of activation areas that respond the one independent component: the primary visual cortex. Although this method can identify the voxels of these areas that have synchronal response to our paradigm, it cannot uncover the relationship between the two activation areas. The

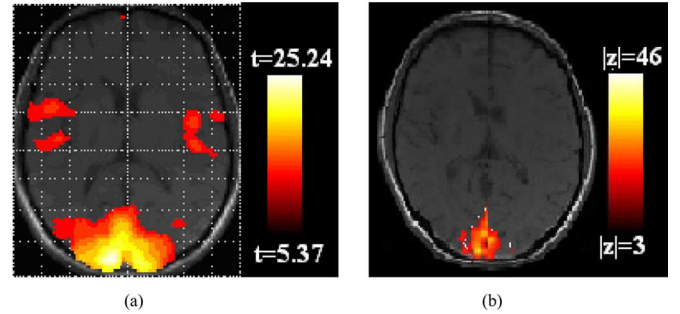


Fig. 10. (a) Visual and motor areas are activated synchronously by SPM. (b) Primary visual cortex is activated by ICA that responds the one independent component.

identified responses to the paradigm are not the same [Fig. 5(d)]; SOM can cluster the two activated areas into individual clusters because of the similarity of the time course of the voxels in these areas. These results further demonstrate that fMRI signal intensity should not be normalized in task fMRI experiments, while normalized signal in a resting fMRI experiment is feasible for the SOM algorithm.

D. Differences in the Dynamic Response

In a multitask fMRI experiment, the brain response to synchronous visual and motor tasks would exist in the delay response; the brain response to a stimulus is approximately equal to the convolution of the input paradigm with the HRF. Note that the convolution task accounting for brain activation responded slowly to stimulus. Precise and robust estimation of the HRF remains a topic of ongoing research, and various methods have been devised with this in mind [51]. A number of functions have been proposed to model the HRF: the Poisson function [49], the Gaussian function [52], and a difference of two gamma-variants functions [53]. In investigating the different brain response to different tasks or stimuli that occur synchronously, the HRF alone does not adequately reveal the actual brain activation response; however, the SOM algorithm (model free) can cluster fMRI time course data using its inherent character and does not

depend on the HRF model. Delay correlation was computed between the paradigm reference and supercluster time course of Cluster 1 in Fig. 5(d), which denotes the brain response in the primary visual cortex. The maximum CC is 0.8785, with delay of three sample points. In light of the above delay in the correlation method, the supercluster time course [Cluster 1 in Fig. 6(d)] of the primary motor cortex in the other slice with paradigm has a maximum CC of 0.8964, with delay of two sample points. The single HRF model cannot synchronously obtain the two brain responses that gain high CCs. Therefore, the SOM clustering method that combines time delay information and stimulus-task-related neuro-anatomical knowledge enables even more information to be obtained than that possible using an image map or paradigm.

E. Event-Related Experiment

It might initially seem that the maximum CCs were much lower than the threshold of statistical significance for the delay correlation method between the supercluster time course of the visual cortex [Fig. 7(e)] and the paradigm [first row signal in Fig. 1(d)] in the event-related experiment. Because the CNR of the fMRI signal in the event-related experiment was lower than that in the block-design experiment, the maximum CC was 0.2221, with a delay of four sample points that were computed between the signals in Fig. 7(e) and the experiment pattern shown by first row signal in Fig. 1(d). The core of the event-related experiment was that based on a single stimulus or behavior event that triggered a hemodynamic response; BOLD signal increasingly achieved pitch when the stimulus occurred, before decreasing to the baseline level. The fact is that use of sample correlation analysis or the *t*-test for event-related fMRI data does not provide satisfactory results; conversely, SOM can detect and cluster these data sets.

F. Functional Connectivity

Recent studies have examined “functional connectivity,” defined as the temporal correlation between spatially remote neurophysiological events [54], to manifest the interaction of a continuous task or spontaneous neuronal activity at rest [55], [56]. This spontaneous brain activity has been studied by correlating low-frequency fluctuations (LFF) in human fMRI signal to investigate potential functional connectivity [57]. Methodological approaches to the study of connectivity can vary broadly; for example, seed-voxel correlation mapping that is dependent on a prior information is one of the simplest techniques [58]; ICA that does not require a prior information is perhaps the second-most popular technique [59]; and hierarchical clustering and SOM are useful for visualizing the relationships between large numbers of regions [60], [61]. Other confounding factors that could contribute to LFF include motion, motion correction, linear detrending, respiration, cardiac harmonics, and cerebrospinal fluid (CSF) pulsation, which account for a significant fraction of the spontaneous BOLD variance in human data [62]–[64]. On this basis, we performed some preprocessing in the present study prior to SOM analysis, including motion correction and linear detrending. Otherwise, SOM as data-driven analysis could cluster the fMRI data into a homogeneous group

that could possibly indicate these confounding factors based on the similarity of BOLD signal. Is preprocessing necessary in data-driven analysis? Can intrinsic functional connectivity be revealed directly using our method? We will investigate this issue in future work.

G. Comparison Our Method With SPM and ICA

In dataset BS1, we used variability in the shape of the hemodynamic response to a stimulation block in block-design data to test the detection ability of conventional SPM, ICA, and the improved SOM method. SPM results show that it is insufficient to use only one reference signal because regression detects multiple active sources. In particular, one assumed active region was not found by the corrected SPM results [Fig. 2(b)]. Because one reference can accurately model a single active source, it cannot serve synchronously as all regressions. The ICA results showed that two independent regions were found, instead of three activation regions. “B.C” and “D” regions were detected as one independent component [Fig. 2(c)]. The temporal component with the reference signal of the “B.C” region had a CC of 0.8681, and that with reference signal of “D” region had a CC of 0.9277 (see Table I). In the case that the assumption that the source signal must be a mutually independent condition is not satisfied, the detection ability of the ICA method decreases [27]–[29]. The SOM results show that our improved method is insensitive to form variations in the hemodynamic response.

In dataset BS2, the SPM method did not find region “D,” whose time course lagged the reference signal, regarding both uncorrected and corrected results [Fig. 3(b)]. This result shows that temporal fMRI series are highly sensitivity to delay [65], [66] if we use only one reference signal as regression. One temporal component of ICA results with reference signal in the “B.C” region has a CC of 0.6792, and with reference signal in the “D” region has a CC of 0.9455 (see Table I). Although the time courses of the “B.C” and “D” regions show an obvious time lag, the assumed independence of ICA is a stronger condition than uncorrelatedness [67]; therefore, the ability of detection and the CC both decrease. Conversely, our method, which does not require a strong prior assumption regarding the delay of the neuronal response, is clearly insensitive to timing variation in the hemodynamic response. The results are similar for BS4.

In block-design simulation data BS3, the performance of our method was inferior to SPM and ICA when CNR was very low, but reached similar levels of performance as the other methods when CNR was higher than 0.75 [Fig. 9(c)]. In event-related simulation data BS5, the performance of our method was inferior to that of SPM and ICA when CNR was very low, but reached similar levels of performance as the other two methods when CNR was higher than 1.25 [Fig. 9(e)].

H. Application and Limitation of the Method

SPM based on GLM requires determinate statistical inference and hypothesis tests that would be form, timing variation in the hemodynamic response. When we investigated multiple active sources, we found that the SPM method requires multiple regression parameters to accurately model the hemodynamic

response. ICA, a data-driven method, requires a strong independency assumption, and remains limited in terms of selecting from among a large number of components.

Improved SOM and HC, another data-driven method, do not require prior knowledge about experimental designs and do take advantage of the intrinsic underlying information in fMRI data. There are some limitations in our method: the HC step may not be necessary if the number of nodes in the SOM lattice is appropriately selected and spatial information is included in constructing weight vectors in SOM training. Furthermore, HC may not show obvious advancement because of the low dimensionality of trained SOM weights.

V. CONCLUSION

In this paper, we proposed a method that integrates improved SOM and HC in detecting and classifying brain activation. The validity of this algorithm was tested by a simulation study and real fMRI data, both of which included block-design and event-related experiments. The results show that the new integrated algorithm can identify activities that arise from different signal sources, other noise sources such as head motion, and different response patterns that arise from simultaneous stimulus tasks.

REFERENCES

- [1] S. Ogawa, T. M. Lee, A. R. Kay, and D. W. Tank, "Brain magnetic resonance imaging with contrast dependent on blood oxygenation," *Proc. Nat. Acad. Sci.*, vol. 87, pp. 9868–9872, 1990.
- [2] K. K. Kwong, J. W. Belliveau, D. A. Chesler, I. E. Goldberg, R. M. Weisskoff, B. P. Poncelet, D. N. Kennedy, B. E. Hoppel, M. S. Cohen, R. Turner, H. Cheng, T. J. Brady, and B. R. Rosen, "Dynamic magnetic resonance imaging of human brain activity during primary sensory stimulation," *Proc. Nat. Acad. Sci.*, vol. 89, pp. 5675–5679, 1992.
- [3] P. A. Bandettini, E. C. Wong, R. S. Hinks, R. S. Tikofsky, and J. S. Hyde, "Time course EPI of human brain function during task activation," *Magn. Reson. Med.*, vol. 25, pp. 390–397, 1992.
- [4] J. Frahm, K. Merboldt, and W. Hancin, "Functional MRI of human brain activation at high spatial resolution," *Magn. Reson. Med.*, vol. 29, pp. 139–144, 1992.
- [5] K. K. Kwong, "Functional magnetic resonance imaging with echo planar imaging," *Magn. Reson. Q.*, vol. 11, pp. 1–20, 1995.
- [6] W. Richter, P. M. Andersen, A. P. Georgopoulos, and S.-G. Kim, "Time-resolved fMRI of mental rotation," *Neuroreport*, vol. 8, pp. 3697–3672, 1997.
- [7] B. R. Rosen, R. L. Buckner, and A. M. Dale, "Event-related functional MRI: past, present and future," *Proc. Nat. Acad. Sci.*, vol. 95, pp. 773–780, 1998.
- [8] J. Xiong, J.-H. Gao, J. L. Lancaster, and P. T. Fox, "Assessment and optimization of functional MRI analyses," *Hum. Brain Mapp.*, vol. 4, pp. 153–167, 1996.
- [9] K. Worsley and K. J. Friston, "Analysis of fMRI time-series revisited—Again," *NeuroImage*, vol. 2, pp. 173–181, 1995.
- [10] P. McCullagh and J. A. Nelder, "Generalized linear models," in *Number 37 in Monographs on Statistics and Applied Probability*, 2nd ed. London: Chapman & Hall, 1989.
- [11] J. Baker, R. Weisskoff, C. Stem, D. Kennedy, A. Jiang, K. Kwong, L. Kolodny, T. Davis, J. Boxerman, B. Buchbinder, V. Wedeen, J. Belliveau, and B. Rosen, "Statistical assessment of functional MRI signal change," in *Proceedings of the 2nd Annual Meeting of the Society of Magnetic Resonance*, 1994, p. 626.
- [12] P. A. Bandettini, A. Jesmanowicz, E. C. Wong, and J. S. Hyde, "Processing strategies for time-course data sets in functional MRI of the human brain," *Magn. Reson. Med.*, vol. 30, pp. 161–173, 1993.
- [13] X. Golay, S. Kollias, D. Meier, A. Valavanis, and P. Boesiger, "Fuzzy membership vs. probability in cross correlation based fuzzy clustering of fMRI data," in *Third International Conference on Functional Mapping of the Human Brain. NeuroImage*, Friberg, Ed. et al., 1997, vol. 3, p. S481.
- [14] M. Razavi, T. J. Grabowski, W. P. Vispoel, P. Monahan, S. Mehta, B. Eaton, and L. Bolinger, "Model assessment and model building in fMRI," *Hum. Brain Mapp.*, vol. 20, pp. 227–238, 2003.
- [15] K. J. Friston, P. Jezzard, and R. Turner, "Analysis of function MRI time series," *Hum. Brain Mapp.*, vol. 1, pp. 153–171, 1994.
- [16] N. Lange and S. L. Zeger, "Non-linear Fourier analysis of magnetic resonance functional neuroimage time series," *Applied Statistics*, vol. 46, pp. 1–29, 1996.
- [17] G. M. Boynton, S. A. Engel, G. H. Glover, and D. J. Heeger, "Linear systems analysis of functional magnetic resonance imaging in human V1," *J. Neurosci.*, vol. 16, pp. 4207–4221, 1996.
- [18] B. Biswal, A. Pathak, B. D. Ward, J. L. Ulmer, K. M. Donahue, and A. G. Hudetz, "Decoupling of the hemodynamic delay from the task induced delay in fMRI," *NeuroImage*, vol. 11, p. S663, 2000.
- [19] F. M. Miezin, L. Maccotta, J. M. Ollinger, S. E. Petersen, and R. L. Buckner, "Characterizing the hemodynamic response: effects of presentation rate, sampling procedure, and the possibility of ordering brain activity based on relative timing," *NeuroImage*, vol. 11, pp. 735–759, 2000.
- [20] R. L. Buckner, P. A. Bandettini, K. M. O'Craven, R. L. Savoy, S. E. Petersen, M. E. Raichle, and B. R. Rosen, "Detection of cortical activation during averaged single trials of a cognitive task using functional magnetic resonance imaging," *Proc. Nat. Acad. Sci.*, vol. 93, pp. 14878–14883, 1996.
- [21] X. Hu, T. H. Le, and K. Ugurbil, "Evaluation of the early response in fMRI in individual subjects using short stimulus duration," *Magn. Reson. Med.*, vol. 37, pp. 877–884, 1997.
- [22] C. E. Curtis, M. W. Cole, V. Y. Rao, and M. D'Esposito, "Canceling planned action: an fMRI study of countermanning saccades," *Cereb. Cortex*, vol. 15, pp. 1281–1289, 2005.
- [23] G. Marrelec, H. Benali, P. Ciuciu, M. Pelegrini-Issac, and J. B. Poline, "Robust Bayesian estimation of the hemodynamic response function in event-related BOLD fMRI using basic physiological information," *Hum. Brain Mapp.*, vol. 19, pp. 1–17, 2003.
- [24] J. J. Sychra, P. A. Bandettini, N. Bhattacharya, and Q. Lin, "Synthetic images by subspace transforms I. Principal components images and related filters," *Med. Phys.*, vol. 21, pp. 193–201, 1994.
- [25] W. Backfrieder, R. Baumgartner, M. Samal, E. Moser, and H. Bergmann, "Quantification of intensity variations in functional MR images using rotated principal components," *Phys. Med. Biol.*, vol. 41, pp. 1425–1438, 1996.
- [26] M. J. McKeown, T.-P. Jung, S. Makeig, G. G. Brown, S. S. Kindermann, T.-W. Lee, and T. J. Sejnowski, "Spatially independent activity patterns in functional magnetic resonance imaging data during the stroop color naming task," *Proc. Nat. Acad. Sci.*, vol. 95, pp. 803–810, 1998.
- [27] M. J. McKeown, S. Makeig, G. G. Brown, T.-P. Jung, S. S. Kindermann, A. J. Bell, and T. J. Sejnowski, "Analysis of fMRI data by blind separation into independent spatial components," *Hum. Brain Mapp.*, vol. 6, pp. 160–188, 1998.
- [28] H. Chen, D. Yao, Y. Zhou, and L. Chen, "Analysis of fMRI data by blind separation of data in a tiny spatial domain into independent temporal component," *Brain Topography*, vol. 15, pp. 223–232, 2003.
- [29] H. Chen and D. Yao, "Discussion on the choice of separated component in fMRI data analysis by spatial independent analysis," *Magn. Reson. Imag.*, vol. 22, pp. 827–833, 2004.
- [30] X. Ding, J. Tkach, P. Ruggieri, and T. Masaryk, "Analysis of time course functional MRI data with clustering method without the use of reference signal," in *Proceedings of the Second Annual Meeting of the International Society for Magnetic Resonance in Medicine*, San Francisco, USA, 1994, p. 630.
- [31] G. Scarth, M. McIntyre, B. Wowk, and R. L. Somorjai, "Detection of novelty in functional images using fuzzy clustering," in *Proceedings of the Second Annual Meeting of the International Society for Magnetic Resonance in Medicine*, San Francisco, USA, 1995, p. 238.
- [32] C. Goutte, P. Toft, E. Rostrup, F. Å. Nielsen, and L. K. Hansen, "On clustering fMRI time series," *NeuroImage*, vol. 9, pp. 298–310, 1999.
- [33] H. Chen, H. Yuan, D. Yao, L. Chen, and W. Chen, "An integrated neighborhood correlation and hierarchical clustering approach of functional MRI," *IEEE Transactions on Biomedical Engineering*, vol. 53, pp. 452–458, 2006.
- [34] H. Fischer and J. Hennig, "Neural network-based analysis of MR time series," *Magnetic Resonance in Medicine*, vol. 41, pp. 124–131, 1999.
- [35] S. C. Ngan and X. Hu, "Analysis of functional magnetic resonance imaging data using self-organizing mapping with spatial connectivity," *Magnetic Resonance in Medicine*, vol. 41, pp. 939–946, 1999.

- [36] K. H. Chuang, M. J. Chiu, C. C. Lin, and J. H. Chen, "Model-Free functional MRI analysis using Kohonen clustering neural network and fuzzy C -means," *IEEE Transactions on Medical Imaging*, vol. 18, pp. 1117–1128, 1999.
- [37] S. C. Ngan, E. S. Yacoub, W. F. Auffermann, and X. Hu, "Node merging in Kohonen's self-organizing mapping of fMRI data," *Artificial Intelligence in Medicine*, vol. 25, pp. 19–33, 2002.
- [38] S. J. Peltier, T. A. Polk, and D. C. Noll, "Detecting low-frequency functional connectivity in fMRI using a self-organizing map (SOM) algorithm," *Hum. Brain Mapp.*, vol. 20, pp. 220–226, 2003.
- [39] T. Kohonen, "The self-organizing map," *Proc. IEEE*, vol. 78, pp. 1464–1480, 1990.
- [40] T. Kohonen, *Self-Organizing Maps*. NY: Springer-Verlag, 1995.
- [41] T. Kohonen, "Comparison of SOM point densities based on different criteria," *Neural Comput.*, vol. 11, pp. 2171–2185, 1999.
- [42] M. Cottrell and P. Rousset, "The Kohonen algorithm: A powerful tool for analyzing and representing multidimensional quantitative and qualitative data," in *IWANN 1997 (International Work-Conference on Artificial Neural Networks)*, 1997, pp. 861–871.
- [43] F. Murtagh, "Interpreting the Kohonen self-organizing feature map using contiguity-constrained clustering," *Pattern Recogn. Lett.*, vol. 16, pp. 399–408, 1995.
- [44] T. Kohonen, "Self-organized formation of topologically correct feature maps," *Biol. Cybernet.*, vol. 43, pp. 59–69, 1982.
- [45] J. Vesanto and E. Alhoniemi, "Clustering of the Self-Organizing Map," *IEEE Transactions on Neural Networks*, vol. 11, pp. 586–600, 2000.
- [46] E. Dimitriadou, M. Barth, C. Windischberger, K. Hornik, and E. Moser, "A quantitative comparison of functional MRI cluster analysis," *Artificial Intelligence in Medicine*, vol. 31, pp. 57–71, 2004.
- [47] P. Skudlarski, R. T. Constable, and J. C. Gore, "ROC analysis of statistical methods used in functional MRI: Individual subjects," *NeuroImage*, vol. 9, pp. 311–329, 1999.
- [48] N. Lange, S. C. Strother, J. R. Anderson, F. A. Nielsen, A. P. Holmes, T. Kolenda, R. Savoy, and L. K. Hansen, "Plurality and resemblance in fMRI data analysis," *NeuroImage*, vol. 10, pp. 282–303, 1999.
- [49] K. J. Friston, P. Jezzard, and R. Turner, "Analysis of functional MRI time series," *Hum. Brain Mapp.*, vol. 1, pp. 153–171, 1994.
- [50] K. J. Friston, A. P. Holmes, J. B. Poline, P. J. Grasby, S. C. Williams, R. S. Frackowiak, and R. Turner, "Analysis of fMRI time-series revisited," *NeuroImage*, vol. 2, pp. 45–53, 1995.
- [51] G. Marrelec, H. Benali, P. Ciuciu, M. Pelegrini-Issac, and J. B. Poline, "Robust Bayesian estimation of the hemodynamic response function in event-related BOLD fMRI using basic physiological information," *Hum. Brain Mapp.*, vol. 19, pp. 1–17, 2003.
- [52] J. C. Rajapakse, F. Kruggel, and D. Y. von Cramon, "Modeling hemodynamic response for analysis of functional MRI time-series," *Hum. Brain Mapp.*, vol. 6, pp. 283–300, 1998.
- [53] K. J. Worsley, C. H. Liao, J. Aston, V. Petre, G. H. Duncan, F. Morales, and A. C. Evans, "A general statistical analysis for fMRI data," *NeuroImage*, vol. 15, pp. 1–15, 2002.
- [54] K. J. Friston, C. D. Frith, and R. S. Frackowiak, "Time-dependent changes in effective connectivity measured with PET," *Hum. Brain Mapp.*, vol. 1, pp. 69–79, 1993.
- [55] J. Rissman, A. Gazzaley, and M. D'Esposito, "Measuring functional connectivity during distinct stages of a cognitive task," *NeuroImage*, vol. 23, pp. 752–763, 2004.
- [56] M. D. Fox and M. E. Raichle, "Spontaneous fluctuations in brain activity observed with functional magnetic resonance imaging," *Nat. Rev. Neurosci.*, vol. 8, pp. 700–711, 2007.
- [57] M. De Luca, C. F. Beckmann, N. De Stefano, P. M. Matthews, and S. M. Smith, "fMRI resting state networks define distinct modes of long-distance interactions in the human brain," *NeuroImage*, vol. 29, pp. 1359–1367, 2006.
- [58] M. D. Fox, A. Z. Snyder, J. M. Zacks, and M. E. Raichle, "Coherent spontaneous activity accounts for trial-to-trial variability in human evoked brain responses," *Nat. Neurosci.*, vol. 9, pp. 23–25, 2006.
- [59] C. F. Beckmann, M. De Luca, J. T. Devlin, and S. M. Smith, "Investigations into resting-state connectivity using independent component analysis," *Philos. Trans R. Soc. Lond. Biol. Sci.*, vol. 360, pp. 1001–1013, 2005.
- [60] R. Salvador, J. Suckling, M. R. Coleman, J. D. Pickard, D. Menon, and E. Bullmore, "Neurophysiological architecture of functional magnetic resonance images of human brain," *Cereb. Cortex*, vol. 15, pp. 1332–1342, 2005.
- [61] S. Achard, R. Salvador, B. Whitcher, J. Suckling, and E. Bullmore, "A resilient, low-frequency, small-world human brain functional network with highly connected association cortical hubs," *J. Neurosci.*, vol. 26, pp. 63–72, 2006.
- [62] R. J. S. Wise, K. Ide, M. J. Poulin, and I. Tracey, "Resting state fluctuations in arterial carbon dioxide induce significant low frequency variations in BOLD signal," *NeuroImage*, vol. 21, pp. 1652–1664, 2004.
- [63] R. M. Birn, J. B. Diamond, M. A. Smith, and P. A. Bandettini, "Separating respiratory-variation-related fluctuations from neuronal-activity-related fluctuations in fMRI," *NeuroImage*, vol. 31, pp. 1536–1548, 2006.
- [64] T. E. Lund, K. H. Madsen, K. Sidaros, W. Luo, and T. E. Nichols, "Non-white noise in fMRI: Does modeling have an impact?," *NeuroImage*, vol. 29, pp. 54–66, 2006.
- [65] Y. Lu, T. Jiang, and Y. Zang, "Region growing method for the analysis of fMRI data," *NeuroImage*, vol. 20, pp. 455–465, 2003.
- [66] H. Chen, D. Yao, W. Chen, and L. Chen, "Delay correlation subspace decomposition algorithm and its Application in fMRI," *IEEE Transactions. Medical Imaging*, vol. 24, pp. 1647–1651, 2005.
- [67] A. Meyer-Baese, A. Wismueller, and O. Lange, "Comparison of two exploratory data analysis methods for fMRI: Unsupervised clustering versus independent component analysis," *IEEE Transactions on Information Technology in Biomedicine*, vol. 8, pp. 387–398, 2004.